Mixing in thermally stratified nonlinear spin-up with uniform boundary fluxes

Meline Baghdasarian, Arturo Pacheco-Vega, J. Rafael Pacheco, and Roberto Verzicco

Citation: Physics of Fluids (1994-present) **26**, 096602 (2014); doi: 10.1063/1.4895435
View online: http://dx.doi.org/10.1063/1.4895435
View Table of Contents: http://scitation.aip.org/content/aip/journal/pof2/26/9?ver=pdfcov
Published by the AIP Publishing

PHYSICS OF FLUIDS **26**, 096602 (2014)

Mixing in thermally stratified nonlinear spin-up with uniform boundary fluxes

Meline Baghdasarian,[1] Arturo Pacheco-Vega,[1] J. Rafael Pacheco,[2,a)] and Roberto Verzicco[3]
[1]*Department of Mechanical Engineering, California State University, Los Angeles, Los Angeles, California 90032, USA*
[2]*SAP Americas Inc., Scottsdale, Arizona 85251, USA; School of Mathematical and Statistical Sciences, Arizona State University, Tempe, Arizona 85287, USA; and Environmental Fluid Dynamics Laboratories, Department of Civil Engineering and Geological Sciences, The University of Notre Dame, South Bend, Indiana 46556, USA*
[3]*Dipartimento di Ingegneria Meccanica, Universita' di Roma "Tor Vergata", Via del Politecnico 1, 00133, Roma, Italy and PoF, University of Twente, 7500 AE Enschede, The Netherlands*

(Received 16 December 2013; accepted 27 August 2014; published online 15 September 2014)

Studies of stratified spin-up experiments in enclosed cylinders have reported the presence of small pockets of well-mixed fluids but quantitative measurements of the mixedness of the fluid has been lacking. Previous numerical simulations have not addressed these measurements. Here we present numerical simulations that explain how the combined effect of spin-up and thermal boundary conditions enhances or hinders mixing of a fluid in a cylinder. The energy of the system is characterized by splitting the potential energy into diabatic and adiabatic components, and measurements of efficiency of mixing are based on both, the ratio of dissipation of available potential energy to forcing and variance of temperature. The numerical simulations of the Navier–Stokes equations for the problem with different sets of thermal boundary conditions at the horizontal walls helped shed some light on the physical mechanisms of mixing, for which a clear explanation was absent. © *2014 AIP Publishing LLC*. [http://dx.doi.org/10.1063/1.4895435]

I. INTRODUCTION

Stratified spin-up flow is a classical fluid mechanics problem that has received considerable attention in recent years. Spin-up occurs when a fluid in state of solid body rotation experiences a sudden increase in the rotation rate, resulting in the propagation of stresses into the interior. The dynamics of spin-up/down is particularly relevant to large-scale geophysical flows, for example, in situations where wind stresses in the open ocean and coastal regions generate ocean gyres and can result in baroclinic motions prompt to distort the temperature field, generate turbulent mixing, and enable redistribution of heat fluxes.[1–8]

The study of mechanisms leading to efficient mixing has long been appreciated in the context of stratified shear flows[9] and thermal convection.[10–15] For example, shear can increase mixing at stratified interfaces by triggering Kelvin-Helmholtz (K-H) instabilities and can produce turbulence via interaction of Reynolds stresses.[16,17] Turbulence in the ocean can also be generated by other mechanisms, including mean velocity shear, breaking of surface or internal waves, and surface cooling.

Motions associated with upwelling are known to cause localized mixing.[5,18] Since most of the time new water masses are formed at the surface by cooling, and their spin-up is clearly of utility in determining ensuing flow patterns, it will be helpful to understand how the spin of water masses in basins subjected to different thermal boundary conditions affect the mixing. Laboratory

a)Electronic mail: rpacheco@asu.edu

experiments of salt-stratified spin-up in a cylinder have shown qualitative measures of mixing,[19–22] and recent three-dimensional simulations have demonstrated how different sets of thermal boundary conditions at the horizontal walls (adiabatic or fixed temperatures) affect the time of formation of columnar baroclinic vortices.[23] Nevertheless, quantitative measurements of mixing and the physical mechanisms controlling its efficiency in spin-up flows has remained relatively unexplored.

In this paper, we study the spin-up of a thermally stratified flow in a cylindrical container in a numerical setting. In addition to the two sets of thermal boundary conditions (prescribed temperatures at the horizontal walls or adiabatic) considered in Refs. 23 and 24, we include a combination of (i) prescribed temperature at the bottom wall and adiabatic at the top, and (ii) prescribed temperature at the top wall and adiabatic at the bottom. The quest here is to investigate how these different thermal boundary conditions, potentially relevant to ocean flows, affect the conversion of energy, the advection of scalars, and the quality of mixing. Our procedure for characterizing the energy conversions follows that of Ref. 25 and split the potential energy into components. One component is the "background" potential energy which has no capacity to do work, and the other is the "available" potential energy to do work. Two questions we address here are: (i) where the kinetic energy supplied by the spin-up terminates, and (ii) how the quality of mixing can be quantified. In the stratified-mixing community is common practice to define the efficiency of mixing as the ratio of the dissipation of the available potential energy to the sum of rates of kinetic and available potential energies in the system.[9] For this flow configuration, irreversible processes (diabatic) act on large scales at the late stages of flow development, as opposed to the mixing process associated with small scales at the onset of spin-up. We have found that as the flow tends to steady state, the mixing efficiency can have negative values due to numerical noise, and viewing this ratio as a "mixing efficiency" may be misleading. For this reason, quantifying mixing in the initial-value decaying problem must be interpreted very differently, particularly when diffusion dominates. We found useful to include a procedure for determining the quality of mixing based on the variance of temperature[26–28] which is commonly used in chaotic mixing. Furthermore, common belief assumes that the best stirring to create mixing is either turbulent or exhibits chaotic trajectories. However, this optimal stirring depends on the boundary flux configuration. These issues will be addressed in Secs. II and III.

II. GOVERNING EQUATIONS AND THE NUMERICAL SCHEME

Consider a Newtonian fluid of kinematic viscosity ν, thermal diffusivity κ, and coefficient of volumetric expansion α, confined in a cylinder of radius R and height h where the gravity and rotation vectors are collinear, as shown schematically in Figure 1. Initially, the fluid is thermally stratified in the vertical direction, with a temperature difference of ΔT over h. The fluid is spun-up from an initial state $\Omega_i = \Omega(1-\epsilon)$ to a new rotation rate Ω, where $\epsilon = \Delta\Omega/\Omega$ and $\Delta\Omega$ is the change of background rotation. To non-dimensionalize the system we use the flow depth h as the length scale, the inertial time Ω^{-1} as the time scale and ΔT as the temperature scale resulting in six non-dimensional parameters:

$$\begin{aligned}
&\text{Aspect ratio:} && \Gamma = R/h,\\
&\text{Ekman number:} && E = \nu/\Omega h^2,\\
&\text{Froude number:} && F = \Omega^2 h/g,\\
&\text{Burger number:} && B = N/\Omega,\\
&\text{Prandtl number:} && Pr = \nu/\kappa,\\
&\text{Rossby number:} && \epsilon = \Delta\Omega/\Omega,
\end{aligned}$$

where $N = (\alpha g \Delta T/h)^{1/2}$ is the buoyancy frequency. The non-dimensional governing equations, under the Boussinesq approximation, are

$$(\partial_t + \boldsymbol{u}\cdot\nabla)\boldsymbol{u} = -\nabla p + B^2\Theta\boldsymbol{e}_z + 2\boldsymbol{u}\times\boldsymbol{e}_z - F\,B^2\Theta r\boldsymbol{e}_r + E\nabla^2\boldsymbol{u}, \tag{1}$$

$$(\partial_t + \boldsymbol{u}\cdot\nabla)\Theta = Pr^{-1}E\nabla^2\Theta, \qquad \nabla\cdot\boldsymbol{u} = 0, \tag{2}$$

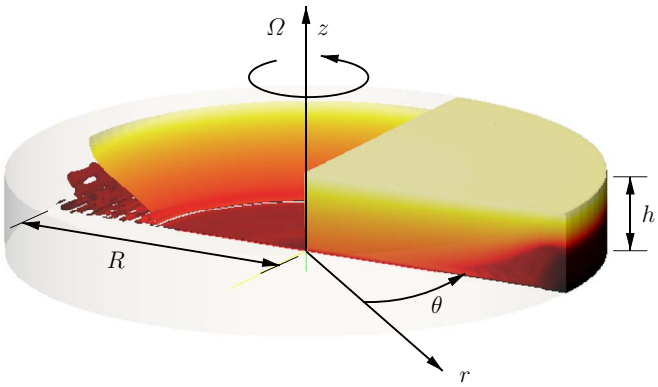

FIG. 1. Schematic of the spin-up seven rotations after the cylinder is accelerated from the initial rotation rate $\Omega_i = \Omega(1-\epsilon)$ to Ω. The left and right quadrants show the vortex core and the accumulation of cold fluid at the bottom corner, respectively.

where $\boldsymbol{u}$ is the velocity field in the rotating frame with components (u, v, w), the cylindrical coordinates (r, θ, z) are the components of $\boldsymbol{r}$, p is the pressure (including gravitational and centrifugal contributions), and Θ is the non-dimensional temperature. The unit vectors in the radial and vertical directions are $\boldsymbol{e}_r$ and $\boldsymbol{e}_z$, respectively. The initial conditions in the rotating frame are $u = w = 0$, $v = -\epsilon\, r$, and $\Theta = z$, the side-wall is no-slip and adiabatic, the top boundary is shear-free, the bottom wall no-slip.

The change in kinetic (E_k), potential (E_p), background potential (E_b), and available potential ($E_a = E_p - E_b$) energy take the form

$$\Delta E_k = \frac{\mathrm{d}}{\mathrm{d}t}\int_V \frac{1}{2}|\boldsymbol{u}|^2 \mathrm{d}V = \int_V \left(B^2\Theta\, w\, - B^2\, F\Theta\, r\, u - E|\nabla \boldsymbol{u}|^2\right)\mathrm{d}V, \tag{3a}$$

$$\begin{aligned}\Delta E_p &= \frac{\mathrm{d}}{\mathrm{d}t}\int_V B^2\left(\frac{1}{B^2\, F} - \Theta\right) z\,\mathrm{d}V = \int_V \left(-B^2\Theta\, w - B^2 Pr^{-1} E\, z\, \nabla^2\Theta\right)\mathrm{d}V,\\ &= \int_V -B^2\Theta\, w\,\mathrm{d}V - B^2\, Pr^{-1} E\int_S z\,\nabla\Theta\cdot\boldsymbol{n}\,\mathrm{d}S\\ &\quad + B^2\, Pr^{-1} E\int_0^{2\pi}\int_0^{\Gamma}[\Theta_T - \Theta_B]\, r\mathrm{d}r\,\mathrm{d}\theta,\end{aligned} \tag{3b}$$

$$\begin{aligned}\Delta E_b &= \frac{\mathrm{d}}{\mathrm{d}t}\int_V B^2\left(\frac{1}{B^2\, F} - \Theta\right) z_R\,\mathrm{d}V\\ &= -B^2 Pr^{-1} E\int_S z_R\nabla\Theta\cdot\boldsymbol{n}\,\mathrm{d}S + B^2 Pr^{-1} E\int_V \frac{\mathrm{d}\, z_R}{\mathrm{d}\,\Theta}|\nabla\Theta|^2\,\mathrm{d}V,\end{aligned} \tag{3c}$$

$$\begin{aligned}\Delta E_a &= \frac{\mathrm{d}}{\mathrm{d}\,t}\int_V B^2\left(\frac{1}{B^2\, F} - \Theta\right)(z - z_R)\,\mathrm{d}V\\ &= \int_V -B^2\Theta\, w\,\mathrm{d}V - B^2\, Pr^{-1} E\int_S (z - z_R)\nabla\Theta\cdot\boldsymbol{n}\,\mathrm{d}S\\ &\quad + B^2\, Pr^{-1} E\int_0^{2\pi}\int_0^{\Gamma}[\Theta_T - \Theta_B]\, r\mathrm{d}r\,\mathrm{d}\theta - B^2\, Pr^{-1} E\int_V \frac{\mathrm{d}\, z_R}{\mathrm{d}\,\Theta}|\nabla\Theta|^2\,\mathrm{d}V.\end{aligned} \tag{3d}$$

Here, $z_R(\Theta, t)$ is the vertical coordinate of the reference state where all the temperature surfaces are horizontal and Θ_T and Θ_B are the temperatures at the top and bottom walls, respectively. The adiabatic reversible vertical buoyancy flux $\Phi_z = \int_V -B^2\Theta\, w\,\mathrm{d}V$, the rate of conversion from internal to potential energy $\Phi_i = B^2\, Pr^{-1} E\int_0^{2\pi}\int_0^{\Gamma}[\Theta_T - \Theta_B]\, r\mathrm{d}r\,\mathrm{d}\theta$, and the surface integral $S_{diff} = -B^2\, Pr^{-1} E\int_S (z - z_R)\nabla\Theta\cdot\boldsymbol{n}\,\mathrm{d}S$ give the rate of change of available potential energy due

to diffusive heat across the boundaries, and $\Phi_d = -B^2\, Pr^{-1} E \int_V \mathrm{d}z_R/\mathrm{d}\Theta |\nabla\Theta|^2\, \mathrm{d}V$ is the rate of change of background potential energy.

The vertical height of the reference state z_R is computed from the probability density function $\lambda(\Theta)$ of the temperature similarly to[29]

$$\lambda(\tilde{\Theta}) = \frac{1}{V}\int_V \delta(\tilde{\Theta} - \Theta)\, \mathrm{d}V. \tag{4}$$

Using the probability density function (4), the reference position $z_R(\Theta)$ yields

$$z_R(\Theta) = 1 - \int_{\Theta}^{\Theta_M} \lambda(\tilde{\Theta})\, \mathrm{d}\tilde{\Theta}, \tag{5}$$

where the nondimensional height of the domain is 1 and Θ_M is the maximum value of the temperature at time t. The potential energy of the reference state E_b can now be obtained from

$$E_b = B^2 \pi \Gamma^2 \int_0^1 \left(\frac{1}{B^2 F} - \Theta\right) z_R\, \mathrm{d}z_R. \tag{6}$$

The mixing efficiency η in a Boussinesq flow is often defined as the ratio between the dissipation part of the available potential energy to that of the sum of the dissipation of E_k and E_a,

$$\eta = \frac{(\Delta E_a)_{diss}}{\Delta E_a + \Delta E_k} = \frac{\Phi_i + S_{diff} + \Phi_d}{\Phi_i + S_{diff} + \Phi_d + \varepsilon}, \tag{7}$$

where the dissipation of E_k is $\varepsilon = -\int_V E|\nabla \boldsymbol{u}|^2 \mathrm{d}V$ and the dissipation part of E_a is $(\Delta E_a)_{diss} = \Phi_z + S_{diff} + \Phi_d$. In the special case of spin-up the initial kinetic energy is provided by the term $\int_V -FB^2\Theta r\, u\, \mathrm{d}V$ and ΔE_k always decreases. Once the flow reaches a final state of solid body rotation, $\Delta E_k = \Delta E_a = 0$.

To solve the governing equations (1) and (2), we employed the fractional-step finite-difference method of Ref. 30. The code has been tested in a wide variety of enclosed cylindrical flows,[23,31–35] establishing resolution requirements over a wide range of parameters. The grid is clustered near the bottom boundary where at least 10 points were placed inside the Ekman layer to have enough resolution near the wall. The typical grid used was $n_\theta \times n_r \times n_z = 96 \times 351 \times 151$. Details about the experimental and numerical test problems used for verification of the numerical code and selection of number of grid points can be found in Ref. 24.

To characterize the departure of the flow from axisymmetry, we quantify the azimuthal disturbances by splitting the variables into nonaxisymmetric and axisymmetric parts. For example, the velocity in (1) can be expressed as $\boldsymbol{u}(r,\theta,z) = \bar{\boldsymbol{u}}(r,z) + \boldsymbol{u}'(r,\theta,z)$, where

$$\bar{\boldsymbol{u}}(r,z) = \frac{1}{2\pi}\int_0^{2\pi} \boldsymbol{u}(r,\theta,z)\, \mathrm{d}\theta. \tag{8}$$

The energy equation for the azimuthal perturbations is obtained after substituting (8) in the momentum equation (1), taking the dot product with $\boldsymbol{u}'$, and integrating over the entire domain V, yielding

$$\Delta E_k' = \frac{\mathrm{d}}{\mathrm{d}t}\int_V \frac{1}{2}|\boldsymbol{u}'|^2 \mathrm{d}V = -\int_V \boldsymbol{u}'\cdot(\boldsymbol{u}'\cdot\nabla\bar{\boldsymbol{u}})\mathrm{d}V - B^2\int_V \Theta\, w'\mathrm{d}V$$
$$+FB^2\int_V \Theta\, ru'\mathrm{d}V - E\int_V |\nabla\boldsymbol{u}'|^2\mathrm{d}V = \sum_{i=1}^{4} h_i. \tag{9}$$

The left-hand-side of (9) represents the kinetic energy growth rate of the azimuthal disturbance due to (h_1) shear of the mean axisymmetric flow (barotropic production); (h_2) conversion of gravitational potential energy (baroclinic production); (h_3) conversion of centrifugal potential energy; and (h_4) viscous dissipation.[32]

This investigation focuses on the regime that corresponds to the transient Ekman bottom boundary layer, based on the criterion of Ref. 36, to determine the region of stability, i.e., $Re_\delta < 55$, where

TABLE I. Boundary conditions used in the simulations.

Case	Bottom wall ($z = 0$)	Top wall ($z = 1$)
PB_PT	$\Theta = 0$	$\Theta = 1$
AB_PT	$\partial\Theta/\partial z = 0$	$\Theta = 1$
PB_AT	$\Theta = 0$	$\partial\Theta/\partial z = 0$
AB_AT	$\partial\Theta/\partial z = 0$	$\partial\Theta/\partial z = 0$

$Re_\delta = U\delta/\nu$ is the Reynolds number referenced to the bottom Ekman layer depth δ and the characteristic velocity $U = \Delta\Omega R$. Laboratory experiments of Ref. 37 showed that the Ekman layer remains stable until $Re_\delta \approx 57$ and becomes fully turbulent at $Re_\delta \geq 150$. Since the parametric studies of Refs. 22, 24, and 38 also showed that for $\Gamma < 1$, the spin-up is less prone to become non-axisymmetric, we then consider large radius to height aspect ratio only, and set $\Gamma = 3.3$. The spin-up is in the nonlinear regime, and we considered three values for Rossby number, i.e., $\epsilon = \{0.5, 0.73, 1\}$. The Ekman number is set at $E = 7.2 \times 10^{-4}$, the Burger number at $B = 2.52$, the Prandtl number at $Pr = 6.85$, and the Froude number at $F = 9.0 \times 10^{-4}$. These values guarantee the flow is in the transient regime, axisymmetric for $\epsilon = 0.5$ and prone to develop columnar vortex structures due to baroclinic instabilities for both $\epsilon = 0.73$ and 1, for the thermal boundary conditions listed in Table I.

We will describe the time-evolution of the solutions in terms of the number of rotations $\tau(= t/2\pi)$ instead of the normalized time t.

III. RESULTS AND DISCUSSION

The contours of temperature shown in Figures 2 and 3 demonstrate that when the flow is spun-up, Ekman transport along the bottom boundary layer transports cold fluid radially outwards and forms well-mixed corner regions that rotate faster than the interior. The isotherms deform and vortex lines tilt in this region, generating an unstable system that can convert potential energy into kinetic energy. The kinetic energy dissipates through friction and reduces the temperature contrast through temperature advection. This is a common feature of the thermally stratified spin-up flow, regardless of the thermal boundary conditions imposed on the horizontal walls.

When the Ekman pumping ceases, the secondary circulation reverses direction and the cold fluid from the corner regions moves back to replace the warm fluid in the core. This occurs about 20 rotations later for PB_PT and PB_AT than for AB_AT and AB_PT. The delay is influenced by the boundary condition at the bottom wall. Notice also that near the adiabatic walls, the fluid that is replaced is nearly homogeneous, whereas near the wall with prescribed temperatures the fluid remains stratified .

The spatio-temporal evolution of temperature along a vertical line at three fixed radii of Figures 4 and 5 shows the formation of "cold" corner regions at $r = 3.2$ and entrainment of warm fluid at $r = 0.05$, both at early times. The cold fluid moves through the Ekman layer radially outwards. The formation of baroclinic waves can be better appreciated around the interface of the core ($r = 1.7$) with about one wave per four rotations until these waves are damped by thermal and viscous dissipation.

The flow behavior for $\epsilon = \{0.5, 0.73\}$ is similar to that of $\epsilon = 1$. The main difference is the time at which the flow becomes three-dimensional, with the transition occurring later for smaller Rossby numbers, but the first baroclinic instability starts seven rotations after spin-up. This is better appreciated from the history profile of azimuthal disturbances h_i. When isothermal boundary conditions are prescribed at the bottom (PB_PT and PB_AT), the development of the flow may be divided into two different stages as shown in Figures 6 and 7 for both $\epsilon = 0.73$ and 1, respectively. The first stage occurs at early times (within 20 rotations) and is characterized by the rise and decay of the baroclinic perturbation. The instability decays due to the increased stratification at the bottom wall where the temperature has been prescribed, i.e., the instability is suppressed and the flow becomes more axisymmetric. The second stage occurs after 20 rotations, in which the flow begins

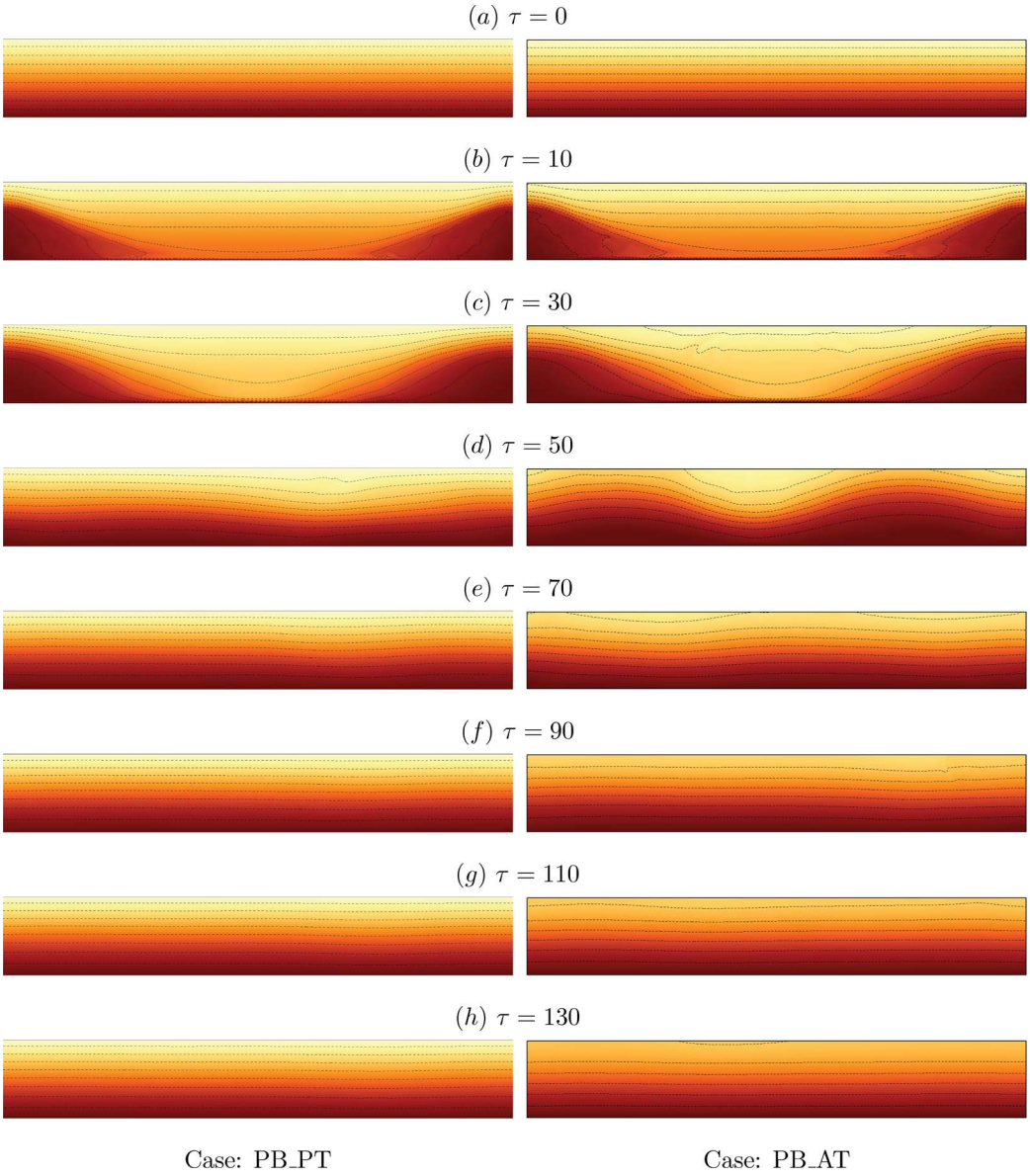

FIG. 2. Contours of temperature Θ on the $r - z$ plane at $\epsilon = 1$. The horizontal dimensions of the cylinder are in Cartesian coordinates $x = [-\Gamma, \Gamma]$ and the vertical is $z = [0, 1]$. At $\tau = 0$, there are 10 linearly spaced contour-levels in the range $\Theta = [0, 1]$. See videos for PB_PT and for PB_AT. (Multimedia view) [URL: http://dx.doi.org/10.1063/1.4895435.1] [URL: http://dx.doi.org/10.1063/1.4895435.2]

to oscillate and breaks into several columnar vortex structures. For adiabatic bottom (AB_AT and AB_PT), after the baroclinic perturbation develops, the vortex-core becomes baroclinically unstable and the flow breaks up into different lenses. Details on how the unstable system develops columnar vortices have been reported in Ref. 24.

One of the main objectives of this study is the quantification of mixing for several types of thermal boundary conditions on the horizontal walls, and the probability density function $\lambda(\Theta)$ is a good indicator of how the temperature is spatially distributed during spin-up. The probability density function $\lambda(\Theta)$ is evaluated numerically by scanning the temperature field, placing its values into bins and normalizing the values by the number of control volumes in each bin. We used two approaches and compared their results. The first consists on interpolating the temperature from the non-uniform grid (r, θ, z) to a uniform Cartesian grid (x, y, z) of size $\Delta x = \Delta y = \Delta z = 0.01$. The

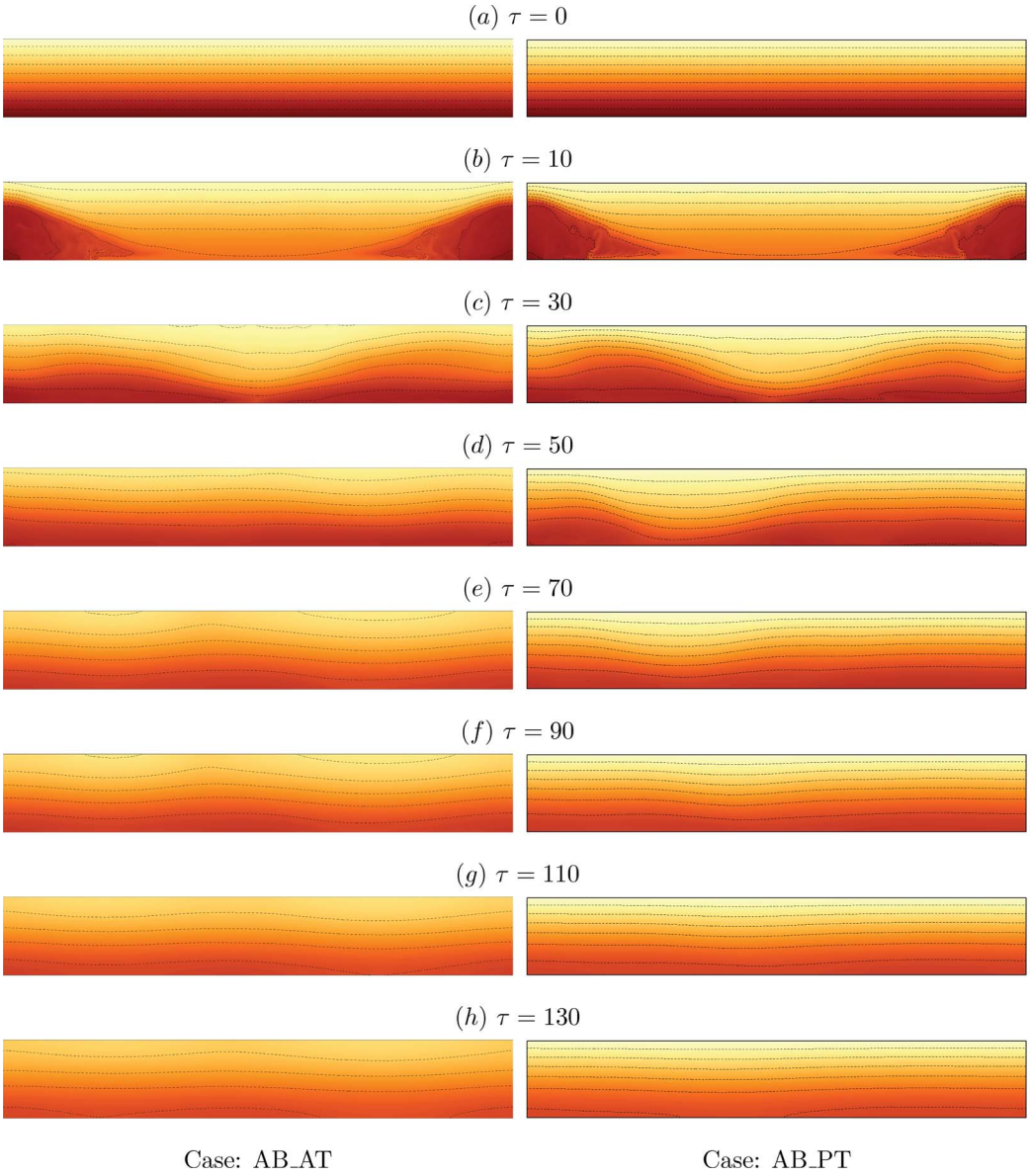

FIG. 3. Contours of temperature Θ on the $r-z$ plane at $\epsilon = 1$. The horizontal dimensions of the cylinder are in Cartesian coordinates $x = [-\Gamma, \Gamma]$ and the vertical is $z = [0, 1]$. At $\tau = 0$, there are 10 linearly spaced contour-levels in the range $\Theta = [0, 1]$. See videos for AB_AT and for AB_PT. [URL: http://dx.doi.org/10.1063/1.4895435.3] [URL: http://dx.doi.org/10.1063/1.4895435.4]

second is by taking the non-uniform grid and use the conditional probability density function in Θ and the volume of the cell, with a number of cells equal to the number of grids $n_\theta \times n_r \times n_z = 96 \times 351 \times 151$. Both approaches have yielded nearly identical results.

Contours of $\lambda(\Theta)$ and cross-sections at various numbers of rotation are shown in Figures 8 and 9, at $\epsilon = 1$, to show the spatio-temporal distribution of temperature for the different sets of boundary conditions considered in this study.

At later times, the linear stratification for PB_PT is almost recovered, whereas for AB_AT, the distribution of temperature is bi-modal, with the asymptotic values of temperature concentrating around the mean $\langle\Theta\rangle = 0.5$. The time evolution of $\lambda(\Theta)$ for PB_AT and AB_PT at $\epsilon = 1$ is shown in Figure 9. For PB_AT, the asymptotic temperature distribution will be $\Theta = 0$ whereas for AB_PT will be $\Theta = 1$.

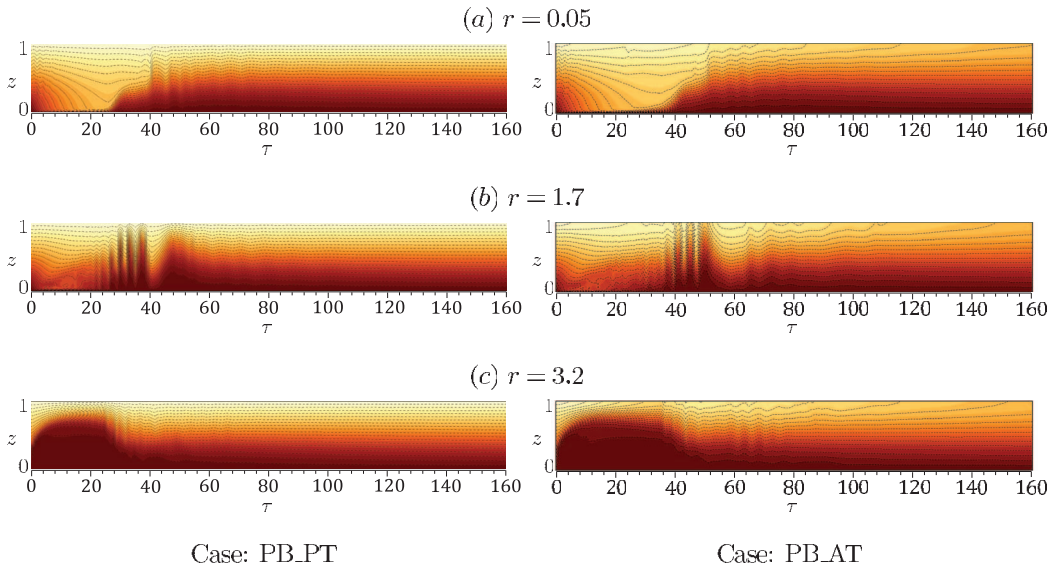

FIG. 4. Spatio-temporal evolution of the temperature along a vertical line at $\theta = 0$ at $\epsilon = 1$ and r as indicated. The horizontal axis indicates time in the range $0 \le \tau \le 160$ and the vertical axis the location of the probes in the range $0 \le z \le 1$. At $\tau = 0$, there are 10 linearly spaced contour-levels in the range $\Theta = [0, 1]$. The figures in the left column correspond to PB_PT, and those in the right column to PB_AT.

The energy rates for $\epsilon = 1$ are shown in Figure 10. Note that the reference energy $\int_V 1/B^2 F \mathrm{d}V$ has been subtracted from the potential and background energies, but not their uniform rate of laminar diffusion, thus emphasizing the energetics associated with the thermal boundary conditions. The kinetic energy driving the motion of the fluid during spin-up is supplied via the centrifugal buoyancy term and it is always positive and decaying. Early in the flow evolution the potential energy increases in all cases due to the positive buoyancy flux Φ_z as shown in Figure 11. This increase in potential energy results from the radial flow through the Ekman layer that pushes the

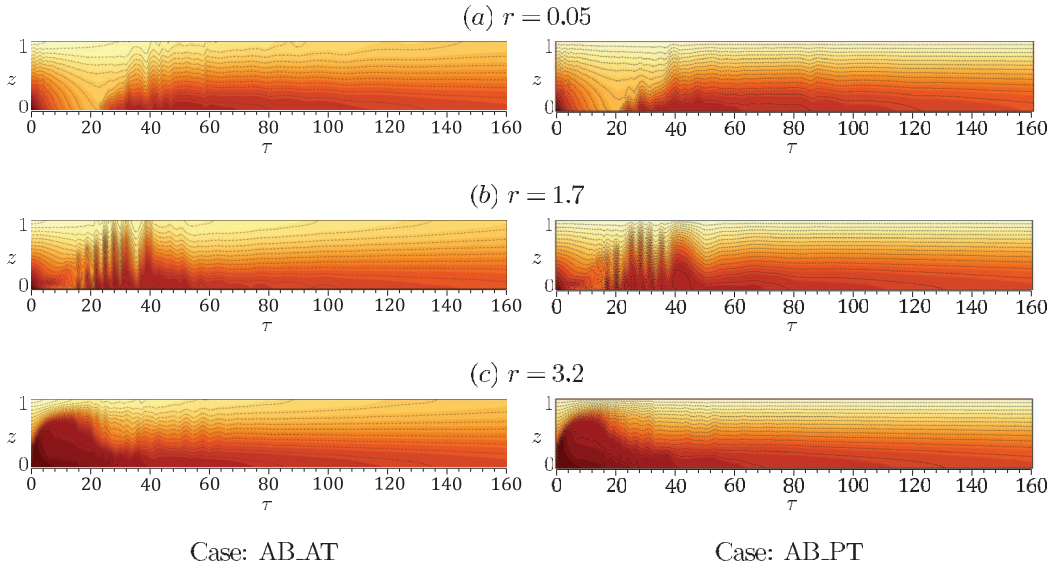

FIG. 5. Spatio-temporal evolution of the temperature along a vertical line at $\theta = 0$ at $\epsilon = 1$ and r as indicated. The horizontal axis indicates time in the range $0 \le \tau \le 160$ and the vertical axis the location of the probes in the range $0 \le z \le 1$. At $\tau = 0$, there are 10 linearly spaced contour-levels in the range $\Theta = [0, 1]$. The figures in the left column correspond to AB_AT, and those in the right column to AB_PT.

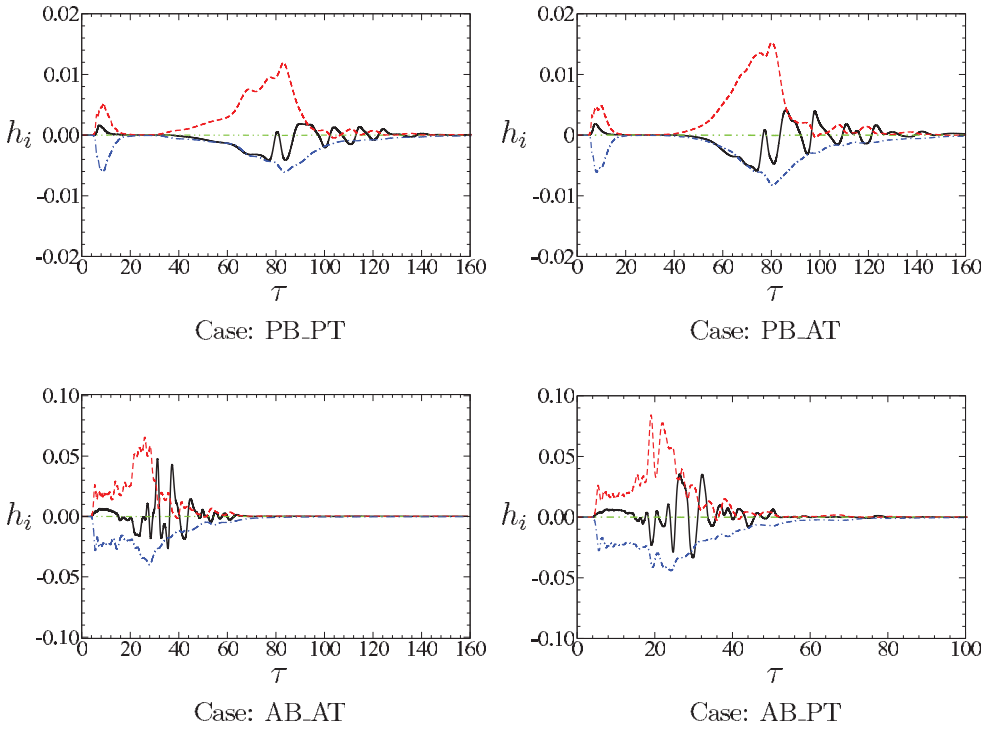

FIG. 6. Time evolution of h_i-terms in the rate of change of kinetic energy of azimuthal perturbations at $\epsilon = 0.73$. Barotropic term h_1 (—— black); baroclinic term h_2 (– – red); centrifugal term h_3 (–· ·– green); and viscous dissipation term h_4 (– · – blue).

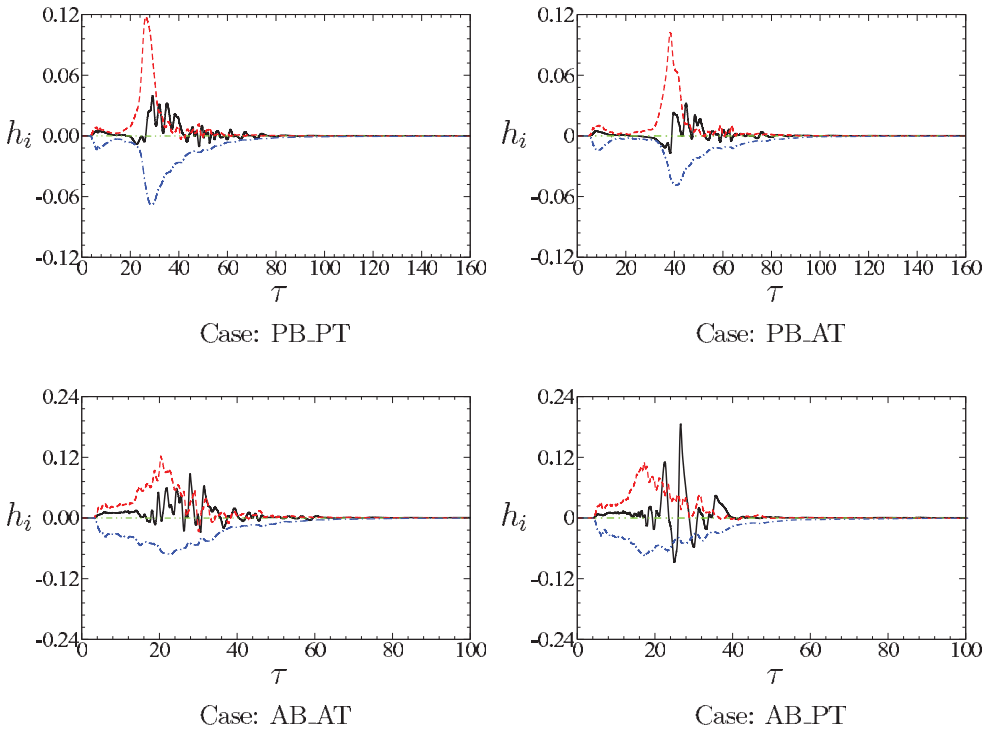

FIG. 7. Time evolution of h_i-terms in the rate of change of kinetic energy of azimuthal perturbations at $\epsilon = 1$. Barotropic term h_1 (—— black); baroclinic term h_2 (– – red); centrifugal term h_3 (–· ·– green); and viscous dissipation term h_4 (– · – blue).

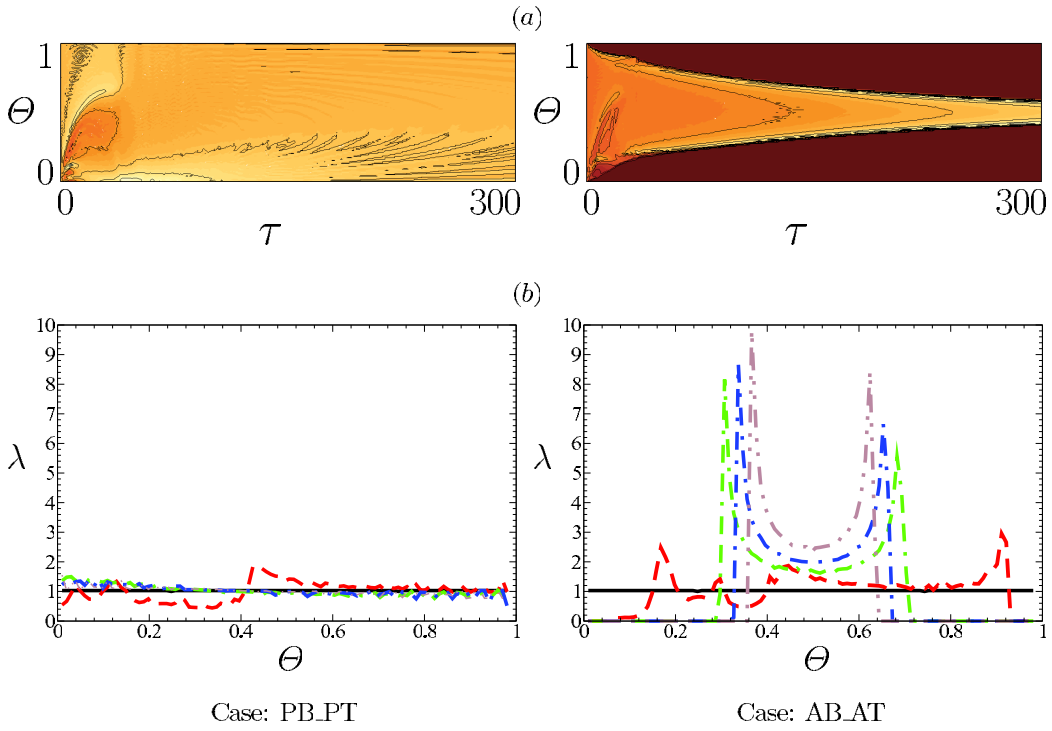

FIG. 8. (a) Contours of probability density $\lambda(\Theta)$ as function of number of rotations τ and (b) cross-sections of λ at: —— (black) $\tau = 0$; – – (red) $\tau = 10$; – – · – – (green) $\tau = 125$; – · – (blue) $\tau = 160$; and – · · · – (brown) $\tau = 200$. The Rossby number is $\epsilon = 1$.

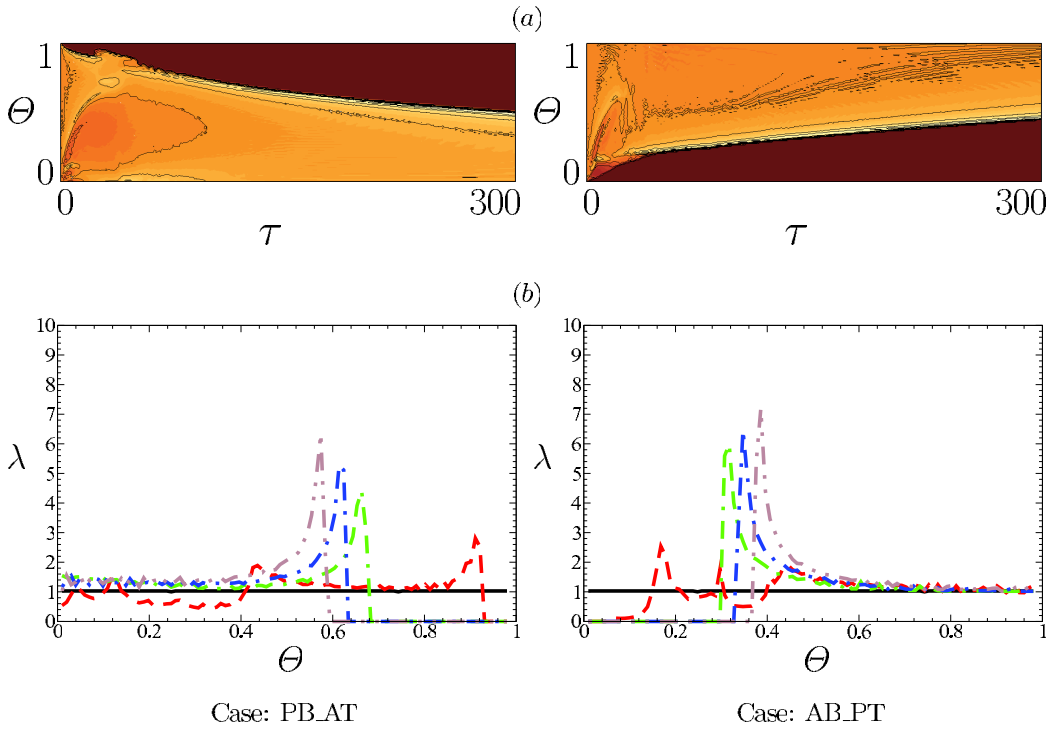

FIG. 9. (a) Contours of probability density $\lambda(\Theta)$ as function of number of rotations τ and (b) cross-sections of λ at: —— (black) $\tau = 0$; – – (red) $\tau = 10$; – – · – – (green) $\tau = 125$; – · – (blue) $\tau = 160$; and – · · · – (brown) $\tau = 200$. The Rossby number is $\epsilon = 1$.

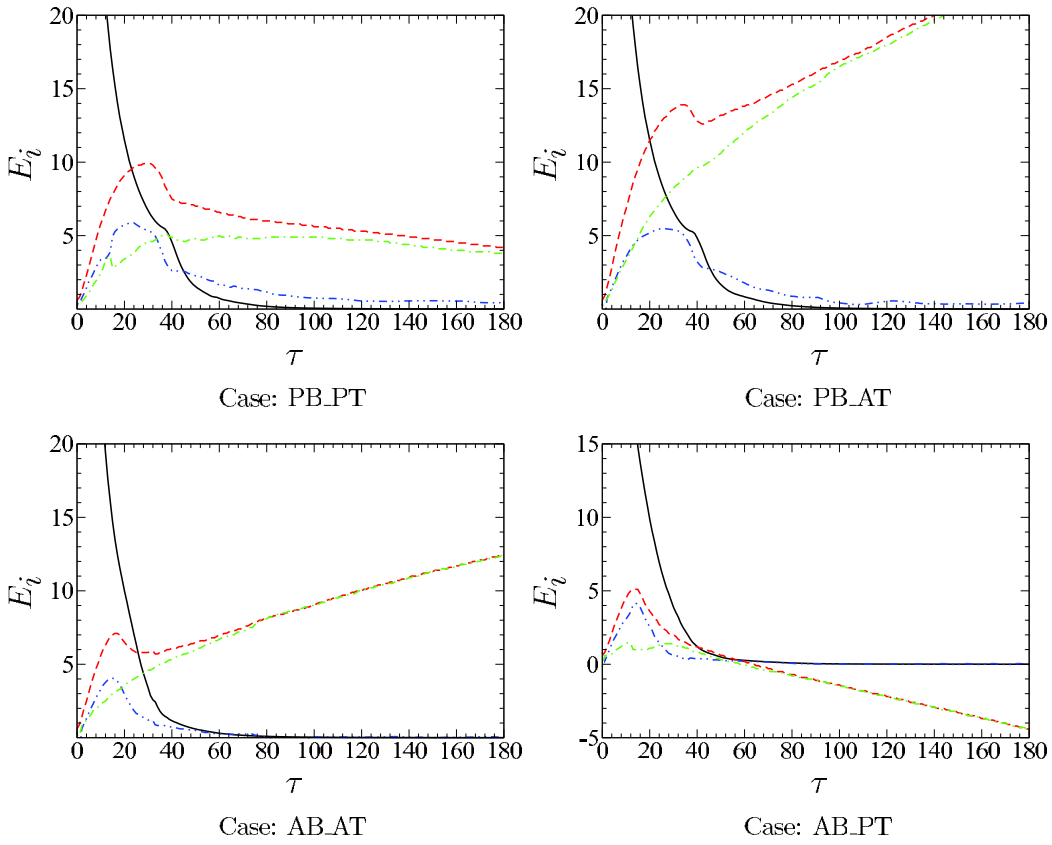

FIG. 10. Time evolution of energies E_i as function of number of rotations τ. Kinetic energy E_k (black ——), potential energy E_p (red – –), background potential energy E_b (green – · –), and available potential energy E_a (blue – · · –). The Rossby number is $\epsilon = 1$.

heavy (cold) fluid to the corner regions. This is a process that occurs between about $\tau = 0$ and 7. How long does the cold fluid remain in the corner regions depends mainly on the bottom boundary condition. The prescribed temperature at the bottom causes a concentration of isotherms parallel to the wall increasing the buoyancy locally and counter-acting the motion of cold fluid from the corner regions back to the core. This is why the buoyancy flux remains positive for a longer number of rotations compared to the adiabatic bottom walls shown in Figure 11. Notice also that Φ_z is maximal and Φ_d is minimal (global for AB_AT and AB_PT and local for PB_PT and PB_AT) at around $\tau = 7$ when the Ekman transport shuts down, but the background potential energy E_b continues to increase due to diffusion as shown in Figure 10. The potential and available potential energies peak at around $\tau = 18$ for AB_AT and AB_PT and around $\tau = 35$ and for PB_PT and PB_AT. This coincides with the global minimal of the buoyancy flux Φ_z for all thermal boundary conditions depicted in Figure 11, where it clearly shows that the magnitude of Φ_d is about two to three times larger than Φ_i. Notice that for adiabatic bottom walls, the magnitude of Φ_d is smaller than the corresponding value when the bottom wall temperatures are prescribed. For a truly turbulent flow $|\Phi_d| \gg \Phi_i$, in our case, it is an indication that the flow is in the laminar regime. This suggests that PB_PT and PB_AT are more laminar than AB_AT and AB_PT.

The term $\Phi_i + S_{diff} + \Phi_d$ indicates the rate of conversion from E_a to E_b in these flows.[15] Note also that the S_{diff} is only slightly different from zero during the spin-up time and its contribution to the energy exchange is relatively small. For $\tau < 60$, most of the conversion from E_a to E_b is accomplished by mixing because $-\Phi_d \gg \Phi_i + S_{diff}$. For $\tau > 60$, $\Phi_d + \Phi_i \approx S_{diff} \approx 0$ owing to the fact that at later times, $E_k \approx E_a \approx 0$ and $E_p \approx E_b$ because vertical motions are suppressed, i.e., the vertical buoyancy flux $\Phi_z = 0$ and the potential energy increases/decreases at the rate of Φ_i.

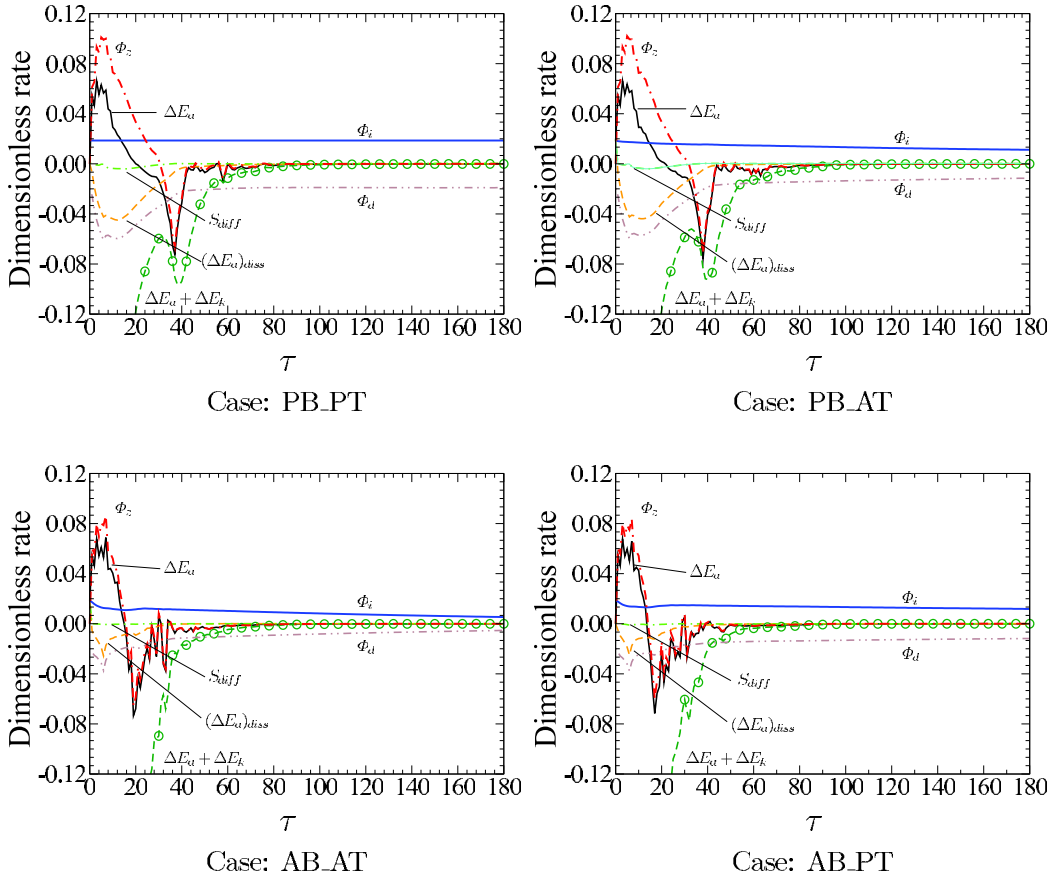

FIG. 11. Rates of energy exchange for the indicated thermal boundary conditions at $\epsilon = 1$.

The effects of boundary conditions on the mixing efficiency is illustrated in Figure 12. For prescribed temperatures at the bottom wall, the mixing efficiency at $\epsilon = 1$ peaks at around $\tau = 28$, which coincides with a local minimum of $|\Delta E_a + \Delta E_k|$, as shown in Figure 11. For $\tau > 60$, the increase and the oscillations of the mixing efficiency are caused by amplified noise due to the smallness of both $(\Delta E_a)_{diss}$ and $\Delta E_a + \Delta E_k \to 0$, when diffusion dominates the scalar transport and vertical motions are absent.

One of the main objectives of this study is the quantification of mixing for several types of thermal boundary conditions on the horizontal walls. As we have seen, the definition of mixing

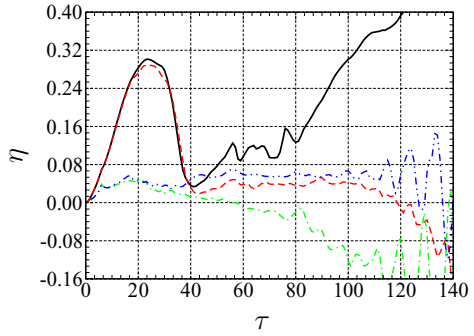

FIG. 12. Time evolution of the instantaneous mixing efficiency η. PB_PT (black ——); PB_AT (red – –); AB_AT (green – · –); and AB_PT (blue – · · –).

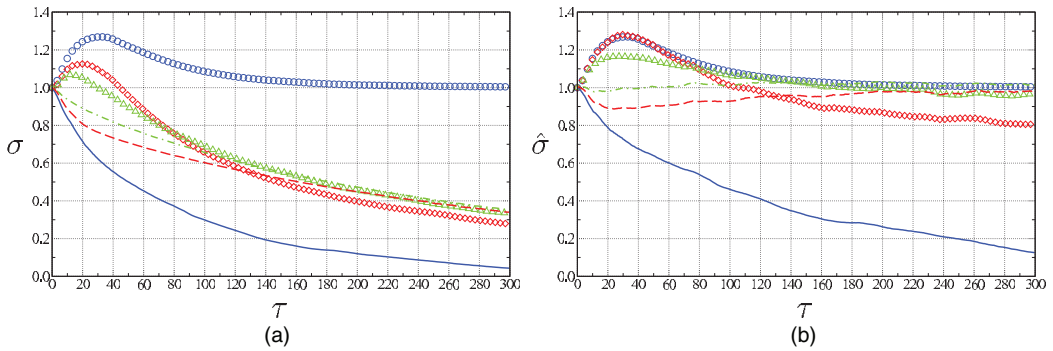

FIG. 13. (a) Variance of temperature σ and (b) modified variance of temperature $\hat{\sigma}$. Δ (green online): PB_AT and $\epsilon = 0.5$; – · – · – (green online): AB_PT and $\epsilon = 0.5$; ○ (blue online): PB_PT and $\epsilon = 1$; — (blue online): AB_AT and $\epsilon = 1$; ◇ (red online): PB_AT and $\epsilon = 1$; and – – – (red online): AB_PT and $\epsilon = 1$.

efficiency as the ratio of the dissipation E_a to forcing $\Delta E_a + \Delta E_k$ is useful only for a time period where the flow is in the transient regime, which is also the interest in spin-up. However, if we are interested in the long-term mixing due to diffusion only, it is useful to introduce a measure of mixing valid for long times, i.e., when the fluid nearly reaches a new state of solid body rotation. A norm that is commonly used to quantify the mixing of the fluid is given by the magnitude of the variance of the scalar Θ,[26–28]

$$\sigma = \frac{\langle \Theta^2(r,\theta,z,t)\rangle - \langle \Theta(r,\theta,z,t)\rangle^2}{\langle \Theta^2(r,\theta,z,0)\rangle - \langle \Theta(r,\theta,z,0)\rangle^2}, \tag{10}$$

where $\langle\cdot\rangle = 1/V \int_V \cdot \mathrm{d}V$. In the presence of boundary fluxes, the norm (10) would reach an asymptotic limit, and normalizing the global measure by the value it would have in the absence of stirring, instead of the initial value, would be more helpful, i.e.,

$$\hat{\sigma} = \frac{\langle \Theta^2(r,\theta,z,t)\rangle}{\langle \hat{\Theta}^2(r,\theta,z,t)\rangle}, \tag{11}$$

where $\hat{\Theta}$ is the temperature due to diffusion only.[39] The temperature $\hat{\Theta}$ is obtained by solving the diffusion problem $\partial_t \hat{\Theta} = Pr^{-1} E \nabla^2 \hat{\Theta}$. Efficient mixing implies $\hat{\sigma} < 1$, if the stirring decreases the variance relative to molecular diffusion alone, which is not always the case when boundary fluxes are present.

For PB_PT the flow mixes locally, but asymptotically, the flow returns to a state of linear stratification, therefore we can expect that this flow will not produce any global mixing. The typical case of an initial value-decaying problem is AB_AT where the final state of mixing is equal to the initial mean. For this case, it is customary to use the variance of temperature to quantify the mixing efficiency. Figure 13(a) shows the variance σ for PB_AT and AB_PT at $\epsilon = 0.5$ and 1. These norms are bounded below by a solid line (AB_AT) and above by circles (PB_PT) representing the best and worst mixing efficiencies (at $\epsilon = 1$), respectively. For prescribed temperature at the bottom wall, the variance increases from its initial value to a maximum and then decreases. The variance is larger in the higher ϵ case due to the more energetic spin-up that pushes more well-mixed cold fluid to the corner regions (compared to the smaller ϵ value), generating a higher temperature contrast with the core. The opposite effect is seen when the bottom wall is adiabatic, i.e., the variance of temperature is lower for $\epsilon = 1$ than for $\epsilon = 0.5$. This is also expected, since the amount of fluid and its temperature (carried to the corner region through the Ekman layer) is larger for the higher value of ϵ. The mixing features mentioned above seem to agree with the flow similarities of PB_AT with PB_PT and AB_PT with AB_AT. The modified variance $\hat{\sigma}$ in Figure 13(b) demonstrates how well the fluid mixes compared to the purely diffusive case for the same conditions as Figure 13(a), where $\hat{\sigma} < 1$ corresponds to efficient mixing. Notice however, that after several tens of rotations the mixing generated by PB_AT is unexpectedly smaller than AB_PT. Surprisingly, at $\tau = 300$ the flow

AB_PT generates as much mixing as the pure diffusion case, and excluding AB_AT, only PB_AT at $\epsilon = 1$ provides $\hat{\sigma} < 1$ for $\tau > 300$.

IV. CONCLUSIONS

In this paper, we have studied numerically the mixing efficiency of spin-up stratified by temperature. Four different combinations of boundary conditions were considered at the bottom/top walls, i.e., prescribed but fixed temperatures, adiabatic or a combination of these two. The kinetic-energy growth-rate of the azimuthal disturbance was used to determine the occurrence of the baroclinic instability. We found that the spin-up with prescribed temperature at the bottom wall and adiabatic top wall was remarkably similar to the flow generated when both temperatures at the horizontal walls were prescribed (PB_PT). Special emphasis was placed on quantifying the mixing in a Boussinesq flow using both, a ratio between the dissipation part of the available potential energy to that of the sum of the dissipation of E_k and E_a, and the variance of temperature (a ratio of the variance to the value it would have without stirring). We have analyzed the energetics of the flow and determined the relationship among the different components for different thermal boundary conditions leading to a better understanding of the spin-up flow. When the temperatures are prescribed on the horizontal walls the asymptotic state recovers its initial stratification, thus the effect of spin-up worsens the global mixing. When the walls are adiabatic, the flow achieves the highest efficiency of mixing. As expected, the mixing efficiency for a flow with prescribed temperature on one wall and adiabatic on the other yielded a mixing efficiency higher than PB_PT but lower than AB_PT.

Since the flow features for AB_PT resembled those of AB_AT, and the latter yielded the highest degree of mixing, we expected that the combination of bottom adiabatic wall and prescribed temperature at the top would render better mixing than PB_AT. This was true only for intermediate times, but asymptotically, PB_AT always performed better than AB_PT (for the same ϵ). This was confirmed by evaluating the potential energy available for mixing for the two flows. During spin-up, the prescribed bottom-wall temperature cooled down the fluid moving radially through the Ekman layer towards the corner regions, creating pockets of cold, but well-mixed fluid, keeping the potential energy available for mixing at a higher level than that obtained through the bottom adiabatic wall. This in turn created higher gradients of temperature, and therefore better mixing for large times.

Several topics of nonlinear spin-up flows remain unexplored that could be potentially important. One of them is how mixing is affected by thermal diffusivity in spin-up. For periods longer than the Ekman spin-up, thermal diffusion is certainly important. If the thermal diffusion is small, the system may take longer time to reach a final state of mixing, whether uniform or linearly stratified, according to the boundary conditions imposed on the horizontal walls. But whether or not a small thermal diffusion will render better mixing for short times is an open question. Further investigation is also needed on the effects of salt-stratification. These two effects are currently being investigated.

ACKNOWLEDGMENTS

M. Baghdasarian is the recipient of a CEaS fellowship, from an NSF HRD-0932421 grant, for which we are grateful. The comments of Steve Wiggins and Alberto Scotti have greatly influenced the final version of this paper and are very much appreciated. We acknowledge the HPC and visualization resources provided by computing centre CASPUR (http://www.caspur.it) and the Ira A. Fulton A2C2 at Arizona State University.

[1] J. S. Allen, "Upwelling and coastal jets in a continuously stratified ocean," J. Phys. Ocean. **3**, 245–257 (1973).
[2] P. F. Linden and G. J. F. van Heijst, "Two-layer spin-up and frontogenesis," J. Fluid Mech. **143**, 69–94 (1984).
[3] T. O. Manley and H. Hunkins, "Mesoscale eddies of the Arctic Ocean," J. Geophys. Res. **90**, 4911–4930, doi:10.1029/JC090iC03p04911 (1985).
[4] J. C. McWilliams, "Submesoscale, coherent vortices in the ocean," Rev. Geophys. **23**, 165–182, doi:10.1029/RG023i002p00165 (1985).
[5] S. Monismith, "An experimental study of the upwelling response of stratified reservoirs to surface shear stress," J. Fluid Mech. **171**, 407–439 (1986).
[6] D. B. Olson, "Rings in the ocean," Annu. Rev. Earth Planet. Sci. **19**, 283–311 (1991).

[7] C. Garrett, P. MacCready, and P. Rhines, "Boundary mixing and arrested Ekman layers: Rotating stratified flow near a sloping boundary," Annu. Rev. Fluid Mech. **25**, 291–323 (1993).
[8] F. Y. Moulin and J.-B. Flór, "On the spin-up by a rotating disk in a rotating stratified fluid," J. Fluid Mech. **516**, 155–180 (2004).
[9] W. R. Peltier and C. P. Caufield, "Mixing efficiency in stratified shear flows," Annu. Rev. Fluid Mech. **35**, 135–167 (2003).
[10] J. S. Turner, *Buoyancy Effects in Fluids* (Cambridge University Press, Cambridge, 1973).
[11] J. S. Turner, "Turbulent entrainment: The development of the entrainment assumption, and its application to geophysical flows," J. Fluid Mech. **173**, 431–471 (1986).
[12] J. J. Sturman, G. N. Ivey, and J. R. Taylor, "Convection in a long box driven by heating and cooling on the horizontal boundaries," J. Fluid Mech. **310**, 61–87 (1996).
[13] T. Maxworthy, "Convection into domains with open boundaries," Annu. Rev. Fluid Mech. **29**, 327–371 (1997).
[14] S. B. Dalziel, M. D. Patterson, C. P. Caufield, and I. A. Coomaraswamy, "Mixing efficiency in high-aspect-ratio Rayleigh-Taylor experiment," Phys. Fluids **20**, 065106 (2008).
[15] K. B. Winters and W. R. Young, "Available potential energy and buoyancy variance in horizontal convection," J. Fluid Mech. **629**, 221–230 (2009).
[16] H. J. S. Fernando, "Turbulent mixing in stratified fluids," Annu. Rev. Fluid Mech. **23**, 455–493 (1991).
[17] E. J. Strang , and H. J. S. Fernando, "Entrainment and mixing in stratified shear flows," J. Fluid Mech. **428**, 349–386 (2001).
[18] J. R. Wells and K. R. Helfrich, "A laboratory study of localized boundary mixing in a rotating stratified fluid," J. Fluid Mech. **516**, 83–113 (10 2004).
[19] J. Pedlosky, *Geophysical Fluid Dynamics* (Springer–Verlag, Berlin, 1987).
[20] H. P. Greenspan, "A note on the spin-up from rest of a stratified fluid," Geophys. Fluid Dyn. **15**, 1–5 (1980).
[21] J.-B. Flór, M. Ungarish, and J. W. M. Bush, "Spin-up from rest in a stratified fluid: Boundary flows," J. Fluid Mech. **472**, 51–82 (2002).
[22] J.-B. Flór, J. W. M. Bush, and M. Ungarish, "An experimental investigation of spin-up from rest of a stratified fluid," Geophys. Fluid Dyn. **98**, 277–296 (2004).
[23] S. A. Smirnov, J. R. Pacheco, and R. Verzicco, "Numerical simulations of nonlinear thermally stratified spin-up in a circular cylinder," Phys. Fluids **22**, 116602 (2010).
[24] J. R. Pacheco and R. Verzicco, "Formation of columnar baroclinic vortices in thermally-stratified non-linear spin-up," J. Fluid Mech. **702**, 265–285 (2012).
[25] K. B. Winters, P. N. Lombard, J. J. Filey, and E. A. D'Asaro, "Available potential energy and mixing in density–stratified fluids," J. Fluid Mech. **289**, 115–128 (1995).
[26] J. L. Thiffeault, "Using multiscale norms to quantify mixing and transport," Nonlinearity **25**, R1–R44 (2012).
[27] J. R. Pacheco, "Mixing enhancement in electro-osmotic flows via modulation of electric fields," Phys. Fluids **20**, 093603 (2008).
[28] J. R. Pacheco, A. Pacheco-Vega, and K. P. Chen, "Mixing-dynamics of a passive scalar in a three-dimensional microchannel," Int. J. Heat Mass Transfer **54**, 959–966 (2011).
[29] Y.-H. Tseng and Joel H. Ferziger, "Mixing and available potential energy in stratified flows," Phys. Fluids **13**, 1281–1293 (2001).
[30] R. Verzicco and P. Orlandi, "A finite-difference scheme for three-dimensional incompressible flows in cylindrical coordinates," J. Comput. Phys. **123**, 402–414 (1996).
[31] R. Verzicco and R. Camussi, "Transitional regimes of low-Prandtl thermal convection in a cylindrical cell," Phys. Fluids **9**, 1287–1295 (1997).
[32] R. Verzicco, F. Lalli, and E. Campana, "Dynamics of baroclinic vortices in a rotating stratified fluid: A numerical study," Phys. Fluids **9**, 419–432 (1997).
[33] S. A. Smirnov, J. R. Pacheco, and R. Verzicco, "Three-dimensional vortex visualization in stratified spin-up," J. Visualization **13**, 81–84 (2010).
[34] J. R. Pacheco, J. M. Lopez, and F. Marques, "Pinning of rotating waves to defects in finite Taylor–Couette flow," J. Fluid Mech. **666**, 254–272 (2011).
[35] J. R. Pacheco, A. Ruiz-Angulo, R. Zenit, and R. Verzicco, "Fluid velocity fluctuations in a collision of a sphere with a wall," Phys. Fluids **23**, 063301 (2011).
[36] D. K. Lilly, "On the instability of Ekman boundary flow," J. Atmos. Sci. **23**, 481–494 (1966).
[37] D. R. Caldwell and C. W. Van Atta, "Characteristics of Ekman boundary layer instabilities," J. Fluid Mech. **44**, 79–95 (1970).
[38] I. Kanda, "A laboratory study of columnar baroclinic vortices in a continuously stratified fluid," Dyn. Atmos. Oceans **38**, 69–92 (2004).
[39] C. R. Doering and J.-L. Thiffeault, "Multiscale mixing efficiencies for steady sources," Phys. Rev. E **74**, 025301 (2006).